

# Microwave Photonic Sensors

Jianping Yao , Fellow, IEEE

(Invited Tutorial)

**Abstract**—Microwave photonics is a field that studies the interaction between microwave and optical waves for the generation, transmission, processing, and measurements of microwave signals by means of photonics, to take advantage of the high speed and broad bandwidth offered by modern photonics. Microwave photonic sensors are one of the active sub-fields that uses microwave photonic techniques to achieve high-speed and high-resolution measurements. In this article, microwave photonic techniques for optical sensing demonstrated in the past few years will be reviewed including high-speed and high-resolution sensing based on heterodyne beating of two optical wavelengths, the use of an optoelectronic oscillator to translate the optical wavelength shift to a microwave frequency change, and the use of wavelength-to-time mapping to translate the sensing information from the optical wavelength domain to the microwave frequency domain, to increase the interrogation speed and resolution. The use of photonic integrated circuits to achieve high-speed and high-resolution microwave photonic sensing will also be discussed.

**Index Terms**—Fiber Bragg grating, fiber optic sensors, microwave photonics, optical heterodyne, optoelectronic oscillator, wavelength-to-time mapping.

## I. INTRODUCTION

FIBER optic sensors have been heavily investigated for the last few decades and numerous techniques have been proposed and demonstrated [1]. It is one of the few fields that has been successfully employed for practical applications such as civil structure health monitoring, biomedical sensing, and quality and process control. In general, an optical sensor is implemented to monitor the wavelength shift due to the change in the environmental conditions, such as the temperature, strain, or vibration. Fiber Bragg gratings (FBGs) have been widely used as optical sensors thanks to the simplicity in implementation due to the fiber nature of the devices which can be inherently incorporated in a fiber-optic link for remote and distributed sensing [2]–[4]. To monitor the wavelength shift, interrogation techniques have been proposed, including directly monitoring the optical spectrum from a sensor using an optical spectrum analyzer (OSA) [2]. It is simple, but it is costly, and the speed is limited, especially for high resolution sensing. The use of an edge filter such as a fiber-optic interferometer [5], [6], to convert

the wavelength or phase change to optical intensity change is another approach that can provide fast interrogation, but the power drifts of the light source or the poor stability of the edge filter will affect the accuracy of the measurements [7], [8]. The use of a fast-scanning optical filter can also realize high-speed and high-resolution interrogation, but the wavelength scanning range is usually limited, or the resolution is compromised if a wider wavelength scanning range is needed [9]. To achieve fast-speed and high-resolution interrogation, one solution is to translate the optical wavelength shift from the optical domain to a microwave frequency shift in the microwave domain, a technique that is called *microwave photonic interrogation* [10], [11]. In this article, optical sensing and interrogation techniques developed in the last few years based on microwave photonics will be reviewed, including heterodyne beating of two wavelengths to generate a microwave signal with its frequency being a function of the sensing information, the use of an optoelectronic oscillator to generate a microwave signal, to translate the optical wavelength shift to the microwave frequency change, and the use of wavelength-to-time (WTT) mapping to translate the sensing information from the optical wavelength domain to the microwave frequency domain, to increase the interrogation speed and resolution. The use of photonic integrated circuits to achieve high-speed and high-resolution microwave photonic sensing will also be discussed.

## II. OPTICAL SENSORS BASED ON A DUAL WAVELENGTH LASER SOURCE

A dual wavelength laser source can be used to implement an optical sensor that has high speed and high resolution. The fundamental concept is to use one wavelength to carry the sensing information while the other wavelength as a reference that is kept unchanged. By beating the two wavelengths at a photodetector (PD), a microwave signal with its frequency change reflecting the wavelength change of the sensing wavelength is generated [11]. By measuring the frequency of the beat signal, the sensing information is obtained at a high speed with high resolution.

Assume that the two wavelengths generated by a dual wavelength laser are given by

$$E_1(t) = E_{01} \cos(\omega_1 t + \phi_1) \quad (1)$$

and

$$E_2(t) = E_{02} \cos(\omega_2 t + \phi_2) \quad (2)$$

where  $E_{01}$ ,  $E_{02}$  are the amplitude terms and  $\phi_1$ ,  $\phi_2$  are the phase terms of the two wavelengths. When the two wavelengths are

Manuscript received October 28, 2020; revised December 17, 2020; accepted December 22, 2020. Date of publication December 25, 2020; date of current version June 16, 2021. This work was supported by the Natural Sciences and Engineering Research Council of Canada (NSERC).

The author is with the Microwave Photonics Research Laboratory, School of Electrical Engineering and Computer Science, University of Ottawa, ON K1N 6N5, Canada (e-mail: jpyao@eecs.uottawa.ca).

This article has supplementary downloadable material available at <https://doi.org/10.1109/JLT.2020.3047442>, provided by the authors.

Digital Object Identifier 10.1109/JLT.2020.3047442

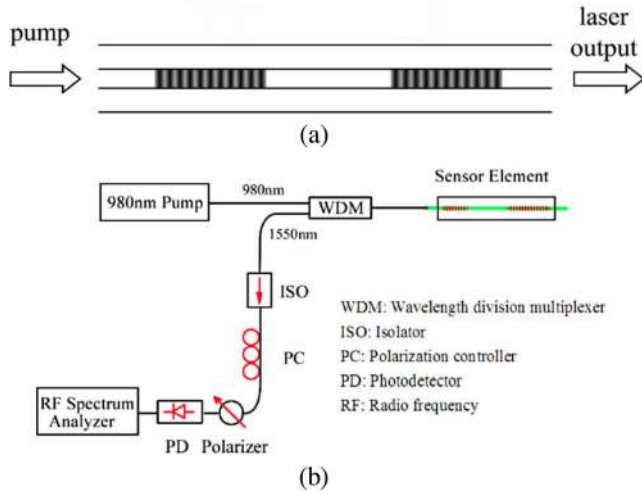


Fig. 1. (a) dual-wavelength DBR laser for high-speed and high-resolution sensing. (b) Beat signal generation and its measurement [12].

applied to a PD, considering the limited bandwidth of the PD, a beat signal with the frequency corresponding to the wavelength difference between the two wavelengths is generated,

$$i_{RF} = A \cos[(\omega_1 - \omega_2)t + (\phi_1 - \phi_2)] \quad (3)$$

where  $A$  is a constant which is determined by  $E_{01}$ ,  $E_{02}$  and the responsivity of the PD. As can be seen, a shift in one wavelength would lead to the change in the beat frequency. For example, at the 1550 nm window, if the wavelength shift is 0.1 pm, the beat frequency will have a change of 12.5 MHz, which can be easily and precisely measured by a digital signal processor (DSP).

A dual-wavelength laser can be implemented using fiber optics. Figure 1(a) shows a dual-wavelength DBR fiber laser with two matched FBGs inscribed in a rare-earth-doped polarization-maintaining (PM) fiber [12]. By controlling the spacing between the two FBGs to make the free spectral range (FSR) greater than the bandwidth of the FBGs, a single longitudinal mode will be supported in the laser cavity, thus mode hopping that is detrimental to the stability of the lasing operation is eliminated. Thanks to the use of a PM fiber, two orthogonal polarization modes are supported with the wavelength spacing determined by the birefringence of the PM fiber. The use of the birefringence of an optical fiber in a laser cavity to generate two orthogonally polarized wavelengths with a wavelength spacing depending on the birefringence has been employed for optical sensing and the approach is known as polarimetric sensing [13], [14]. Compared with the mode hopping between longitudinal modes, the competition between the two polarization modes is much weaker due to polarization-burning-hole effect [15]. As a result, a beat signal with its frequency corresponding to the two polarization modes is generated, which is used to measure the external perturbations.

Assume that the DBR laser operates in single-longitudinal mode with two orthogonally polarized modes, the two lasing wavelengths can be expressed by

$$\lambda_{x,y} = \frac{2n_{x,y}L_{eff}}{M} \quad (4)$$

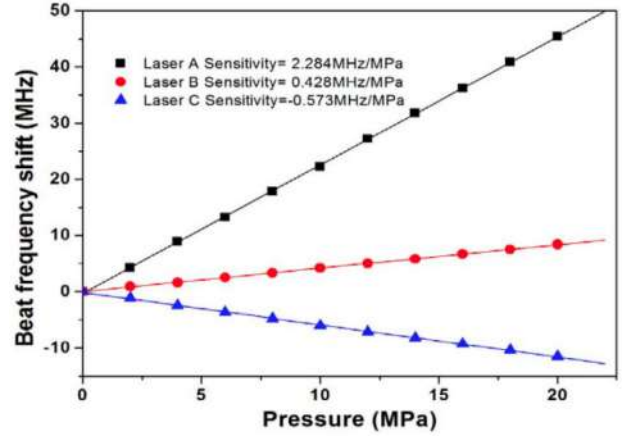


Fig. 2. The beat-frequency change as a function of the applied lateral force for three different DBR lasers [12].

where  $n_{x,y}$  is the effective refractive indices of the two polarization modes corresponding to the two orthogonal polarization directions,  $L_{eff}$  is the effective cavity length, and  $M$  is the order of the longitudinal mode.

By using a polarizer to project the two orthogonally polarized modes to a same polarization direction and applying the two assigned modes to a PD, as shown in Fig. 1(b), a beat signal is generated. The beat frequency is given by

$$f_b = f_x - f_y = \frac{c}{n_0\lambda_0} B \quad (5)$$

where  $n_0$  is the average refractive index of the fiber  $\lambda_0$  is the Bragg wavelength of the FBGs, and  $B = |n_x - n_y|$  is the fiber birefringence.

The use of the DBR laser for lateral force sensing was performed. The lateral force and the beat frequency change has a linear relationship. Fig. 2 shows the beat-frequency change as a function of the applied lateral force for three different DBR lasers. As can be seen that the highest sensitivity is 2.28 MHz/MPa. The resolution is determined by the spectral width of the generated microwave signal. In the experiment [12], the 3-dB bandwidth of the generated microwave signal is 2 kHz, corresponding a very high sensing resolution of 9 kPa.

Similar approach using a dual wavelength DBR laser for temperature and strain sensing was also reported [16]. A strain sensitivity of 0.15 pm/ $\mu\epsilon$  over a range of 0-2400  $\mu\epsilon$  and a temperature sensitivity of 14.3 pm/ $^\circ\text{C}$  over a range of 2 -230  $^\circ\text{C}$  were demonstrated.

An integrated intra-laser-cavity microparticle sensor based on a dual-wavelength distributed-feedback channel waveguide laser in a ytterbium-doped amorphous aluminum oxide on a silicon substrate was also demonstrated [17]. Fig. 3 shows the experimental setup for microparticle sensing. The laser has a Bragg grating in the cavity with two localized quarter wavelength phase shifts, to introduce two resonances that form two longitudinal lasing modes. The wavelength spacing between the two lasing modes is changed due to the particle-induced scattering of laser power, making the population inversion increase, which makes the temperature and refractive index of the waveguide decrease,

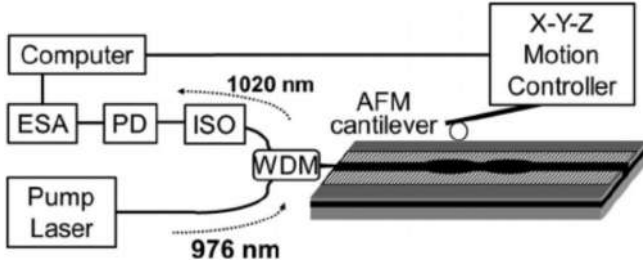
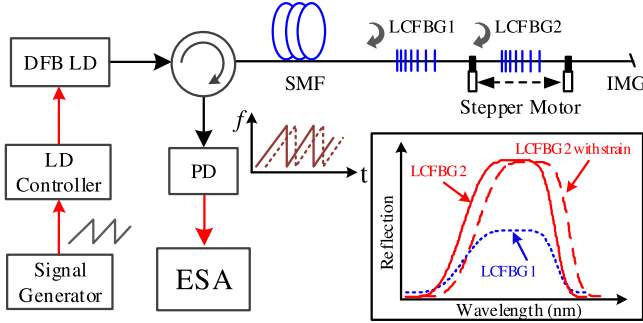
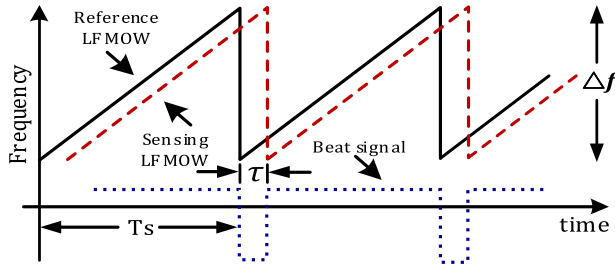


Fig. 3. Intra-laser-cavity micro-particle dual-wavelength laser for microparticle sensing [17].



(a)



(b)

Fig. 4. (a) linearly chirped optical waveform generated by a DFB laser is sent two LCFBGs, to generate two time-delayed linearly chirped optical waveforms. A beat signal between the two time-delayed linearly chirped optical waveforms is generated at the output of the PD. (b) Frequency relationship between the two time-delayed linearly chirped optical waveforms and the corresponding beat frequency [18].

thereby altering the thermal chirp of the Bragg grating in the laser cavity, leading to the change in the frequency spacing between the two lasing modes. The results showed that real-time detection and accurate size measurement of single micro-particles with diameters ranging between 1 and 20  $\mu\text{m}$  were achieved.

Instead of using two single-frequency optical wavelengths to beat to generate a microwave signal, high-speed and high-resolution sensing can also be realized by beating two time-delayed linearly frequency-modulated (or chirped) optical waveforms (LFMOW) [18]. As shown in Fig. 4(a), a linearly chirped optical waveform generated by a frequency-modulated laser diode (LD) is launched into a linearly chirped FBG (LCFBG) pair consisting of two identical LCFBGs with one serving as a sensing LCFBG and the other as a reference LCFBG. The reflection from the two LCFBGs would lead to two time-delayed linearly chirped optical waveforms. By beating the

time-delayed chirped waveforms at a PD, a microwave signal with its beat frequency that is proportional to the time delay difference between the two time-delayed chirped waveforms is generated. By measuring the frequency change of the beat signal, the sensing information is measured [18]. This technique, also called dechirping, has been employed in radar systems for target detection [19]. Fig. 4(b) shows the relationship between two time-delayed linearly chirped optical waveforms. As can be seen the frequency difference between the two waveforms is a function of the time delay. By measuring the beat frequency, the time delay is measured.

For a reference waveform, the instantaneous optical frequency  $\omega_1(t)$  is given by

$$\omega_1(t) = \omega_0 + \alpha t \quad (6)$$

where  $\omega_0$  is the angular frequency at the start of a period of the waveform, and  $\alpha$  is the chirp rate.

The optical field of the reference waveform  $E_1(t)$  can be written as

$$E_1(t) = A_1 \exp \left[ j \left( \omega_0 t + \frac{1}{2} \alpha t^2 + \varphi_0 \right) \right] \quad (7)$$

where  $A_1$  is the amplitude and  $\varphi_0$  is the initial phase of the reference waveform.

Similarly, the optical frequency and the optical field of the time-delayed sensing waveform can be written as

$$\omega_2(t, \tau) = \omega_0 + \alpha(t - \tau) \quad (8)$$

$$E_2(t) = A_2 \exp \left\{ j \left[ \omega_0(t - \tau) + \frac{1}{2} \alpha(t - \tau)^2 + \varphi_0 \right] \right\} \quad (9)$$

where  $A_2$  is the amplitude of the sensing waveform, and  $\tau$  is the time delay difference between the two waveforms, given by,  $\tau = 2n_{eff}L/c$ , where  $L$  is the distance between the two LCFBGs,  $n_{eff}$  is the refractive index of the fiber,  $c$  is the velocity of light in vacuum. When these two waveforms are applied to a high-speed PD, a beat signal is generated, given by

$$\begin{aligned} i(t, \tau) &= R |E_1(t) + E_2(t, \tau)|^2 \\ &= R \left[ I_1 + I_2 + 2\sqrt{I_1 I_2} \cos \left( \alpha\tau t + \omega_0\tau - \frac{1}{2}\alpha\tau^2 \right) \right] \end{aligned} \quad (10)$$

where  $I_1$  and  $I_2$  are the intensities of the reference and sensing signals, respectively, and  $R$  is the responsivity of the PD. As can be seen the beat frequency is  $\alpha\tau$ , which is proportional to the time delay. By measuring the beat frequency, the time delay is measured.

This technique is classified in the category of heterodyne beating since the sensing information is obtained by measuring the beat frequency between two time-delayed chirped waveforms. The advantage of this approach compared with the use of a dual wavelength laser source is its high stability. The stability of a dual wavelength laser is usually poor due to mode competition. This problem is fully solved by beating two time delayed linearly chirped optical waveforms.

### III. OPTICAL SENSORS BASED ON AN OPTOELECTRONIC OSCILLATOR

The wavelength change of an optical sensor can also be translated to microwave frequency change using an optoelectronic oscillator (OEO) [20]. An OEO is a hybrid optical and electronic system that consists of a hybrid amplified feedback loop. Thanks to the use of a long fiber delay line in the loop, the Q factor can be controlled large, which would lead to the generation of a microwave signal with an ultra-low phase noise. An OEO with an ultra-low phase noise can find important applications in communications, radar and instrumentation. This was the original motivation of proposing and implementing of an oscillator using a high Q factor hybrid optoelectronic loop for low phase noise microwave generation. For sensing applications, however, the high Q factor is not a major concern, instead, the stability of microwave generation and the sensitivity of the oscillation frequency to environmental change are the primary concerns.

In general, the oscillation frequency is determined by the center frequency of an optical filter in the hybrid loop. If the wavelength of the optical filter is changing due to the change in the environmental conditions, then the microwave frequency is also changing. By monitoring the microwave frequency, the sensing information is measured. Thus, an optical filter that is sensitive to environmental changes is a critically important device in a sensing OEO. For example, a phase-shifted FBG (PS-FBG) can be used as an optical filter, which can be used for distributed sensing. An integrated ring resonator can also be used as an optical filter, which is particularly useful for microparticle sensing due to the ultra-small size in nature. In the last few years, the use of an OEO for high speed and high-resolution sensing has been well studied and numerous techniques have been reported. In the following, two OEO based sensors that were implemented for strain sensing and for temperature-insensitive lateral force sensing will be discussed.

A high-speed and high-resolution strain sensor based on a tunable OEO employing a phase-shifted FBG (PS-FBG) is shown in Fig. 5(a) [21]. The system consists of a laser diode (LD), a polarization controller (PC), a phase modulator (PM), a PS-FBG, and a PD. A light wave generated by the LD is sent to the PM via the PC. The PC is used to minimize the polarization dependent loss. The phase-modulated light wave is sent to the PS-FBG through an optical circulator (OC) and the reflected optical signal is sent to the PD where a microwave signal is generated. After electronic amplification by an electronic amplifier (EA), the microwave signal at the output of the PD is split into two paths, with one sent to the PM to close the OEO loop and the other sent to a DSP for frequency measurement. Once the loop gain is greater than the loop loss, microwave oscillation will start and a microwave signal with the frequency determined by the center frequency of an equivalent microwave bandpass filter (MBPF) is generated.

The MBPF is implemented by the joint operation of the PM, the PS-FBG, and the PD. As can be seen from Fig. 5(b), one first-order sideband of the phase-modulated optical signal is filtered out by the notch of the PS-FBG. Thus, the phase modulated optical signal is converted to an intensity-modulated optical

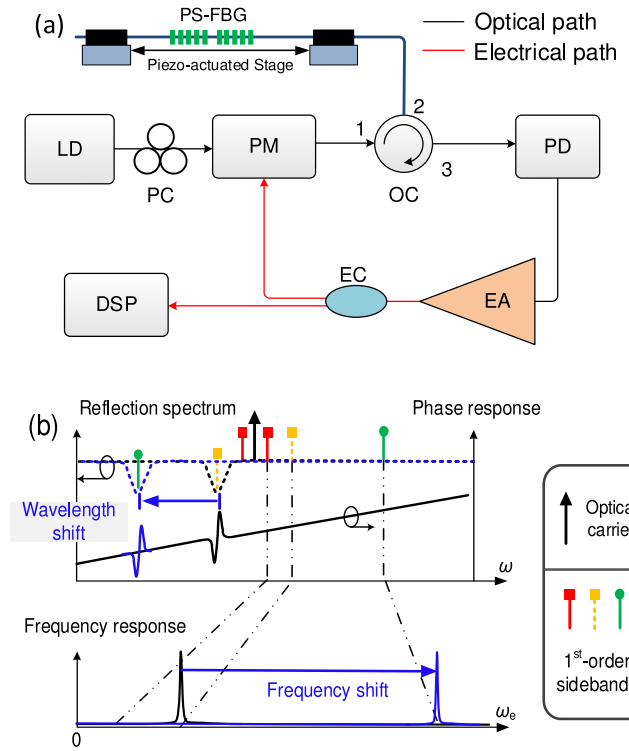


Fig. 5. (a) strain sensor based on an OEO employing a PS-FBG. (b) An equivalent microwave bandpass filter in the OEO [21].

signal, and a MBPF is implemented based on phase-modulation to intensity-modulation (PM-IM). The bandwidth of the MBPF is determined by the notch width of the PS-FBG, which is usually a few tens of MHz. As shown in Fig. 5(b), when the PS-FBG is stretched, the notch wavelength is shifted due to the variation of the grating pitch. As a result, the central frequency of the MBPF is correspondingly shifted. The OEO system would translate the optical wavelength change to a microwave frequency change, and the optical-domain measurement is translated to an electrical spectrum measurement, ensuring a significantly increased measurement speed and resolution. In addition, the use of an oscillatory scheme has also a positive impact on the signal-to-noise ratio (SNR) performance, making the measurement more accurate.

Fig. 6(a) shows the frequency response of the MBPF, which was implemented based on PM-IM in a PS-FBG. The PS-FBG has a bandwidth (full-width at half-maximum or FWHM) of about 30 MHz. Thus, the bandwidth of the MBPF is about 30 MHz. The PS-FBG was fabricated by introducing a phase shift to a uniform FBG during the fabrication process. The PS-FBG was incorporated in the OEO and it was mounted on a piezo-actuated stage for strain measurement. When the OEO loop was closed and the gain is greater than the loss, a microwave signal with a frequency of 10 GHz and a 70-dB sidemode suppression ratio was generated, as shown in Fig. 6(b). The 70-dB sidemode suppression ratio is related to the SNR of the wavelength interrogation scheme, well beyond the achievable values by any other techniques. The phase noise performance of the generated 10-GHz microwave signals is shown in Fig. 6(c). At 10 kHz

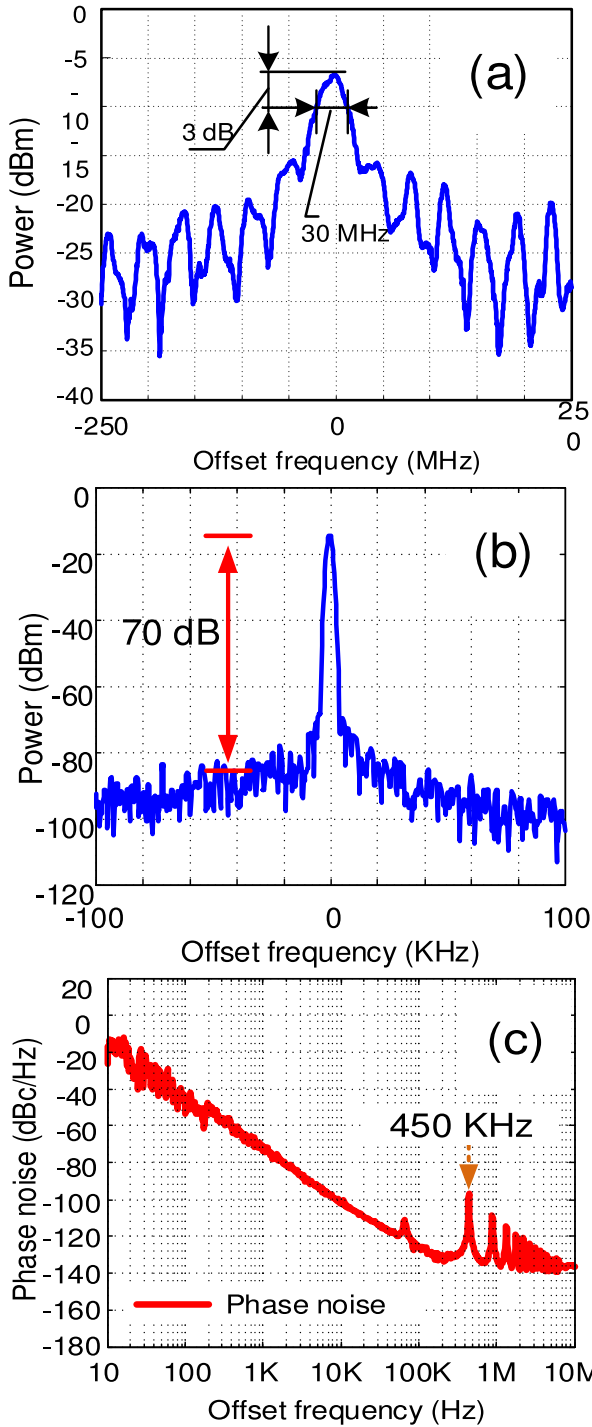


Fig. 6. (a) Frequency response of the microwave bandpass filter. The 3-dB bandwidth is 30 MHz. (b) Spectrum of the 10-GHz microwave signal generated from the OEO. (c) Phase noise measurement of the microwave signal [21].

offset, the phase noise is -105 dBc/Hz, confirming the high phase noise performance of an OEO. Note that multiple peaks are observed at offset frequencies equal or greater than 450 kHz. This value corresponds to the longitudinal mode spacing of the OEO. A shorter OEO loop would make the mode spacing greater, but with poorer phase noise performance. When the notch wavelength of the PS-FBG is shifted, the frequency of the

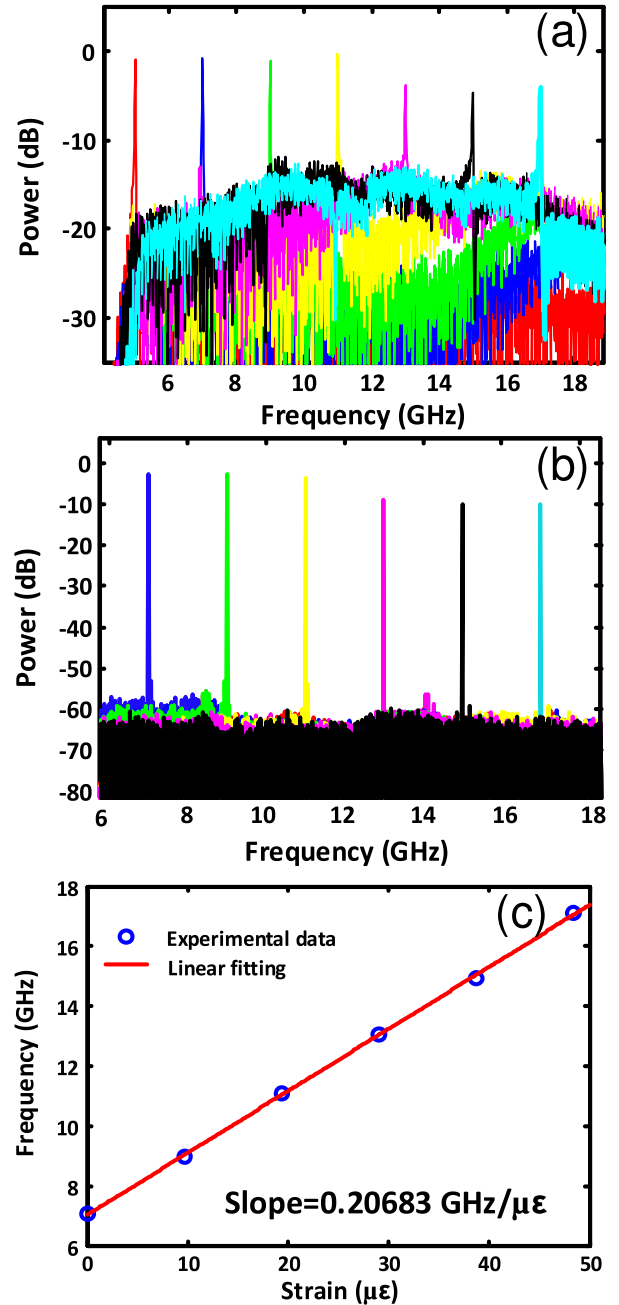


Fig. 7. (a) Measured frequency response of the PS-FBG-based microwave bandpass filter for different applied strains. (b) Spectra of the generated microwave signal at the OEO output for different strains. (c) Relationship between the applied strain and the frequency of the generated microwave signal [21].

generated microwave signal is then shifted accordingly and can be easily measured using a DSP. Fig. 7(a) shows the measured frequency response of the MBPF for different applied axial strains. The spectra of the generated microwave signals at the OEO output corresponding to the different applied strains are shown in Fig. 7(b). The frequency of the generated microwave signal is shifted from about 7 to 17 GHz. The frequency range can be wider if wider bandwidth components are used. The measurements confirm the expected linear relationship between the applied strain and the frequency of the generated microwave signal, as shown in Fig. 7(c).

To make the sensor for lateral force sensing that is insensitive to temperature changes, a transverse load is applied to the PS-FBG to introduce a birefringence, to create two orthogonally polarized notches, which would lead to the generation of two microwave signals at two different frequencies. By beating two microwave frequencies, a third frequency is generated. Since the two microwave frequencies are experiencing the same frequency shift due to temperature change, the third frequency is insensitive to temperature change.

The configuration of an OEO sensor for lateral force sensing that is insensitive to temperature changes is shown in Fig. 8(a) [22]. As can be seen a light wave generated by a laser source is sent to a polarization modulator (PolM) via a polarization controller (PC1). The PolM is a special phase modulator that supports phase modulation along the orthogonal principal axes with complementary phase modulation indices. For simplicity, here we assume that the incident light is aligned with one of the principal axes and thus the PolM is operating as a regular PM. The phase-modulated signal is then sent to the PS-FBG through an OC. One sideband of the phase-modulated signal is removed by the notch of the polarization-maintaining PS-FBG, and the phase-modulated signal is converted to a single-sideband intensity-modulated signal and is detected at a PD. The detected electrical signal is sent back to the PM after amplification by an EA, to close the OEO loop.

When the loop gain is greater than the loop loss, the OEO will start to oscillate, and two microwave signals at different frequencies are generated. The beating between the two microwave signals would generate a third microwave signal (a beat signal) with its frequency being a function of the birefringence. Thus, by measuring the beat frequency, the transverse load applied to the PS-FBG can be measured. Since the two frequencies are experiencing the same temperature change, the third frequency is temperature insensitive.

As shown in Fig. 8(a), when a linearly polarized incident light with an angle of  $45^\circ$  relative to one principal axis of the PolM is sent to the PolM, the light is equally projected to the two orthogonal polarization axes, thus a microwave photonic filter having dual passbands with a band separation of 6 GHz is generated. Fig. 8(b) shows the passband of the microwave photonic filter along the horizontal or vertical polarization direction, measured by aligning the incident light having an angle of  $0^\circ$  or  $90^\circ$  relative to one principal axis of the PolM. Fig. 8(c) shows the filter frequency response when the incident light having an angle of  $45^\circ$  relative to one principal axis of the PolM. A dual pass band filter is realized. When the OEO loop is closed, two microwave signals at two frequencies determined by the two passbands are generated.

Note that due to the nonlinearity of the PolM, a third signal that is the beat note between the two microwave signals is generated, as shown in Fig. 9(a). The frequency of the beat note is directly associated with the birefringence introduced by the transverse load to the PS-FBG. Thus, by measuring the beat frequency, the transverse load is measured. By using the typical values of a silica fiber, we have the relationship between the transverse load the beat frequency, which is given by  $d\nu/dF \approx -9.9\text{GHz}/(\text{N}/\text{mm})$ .

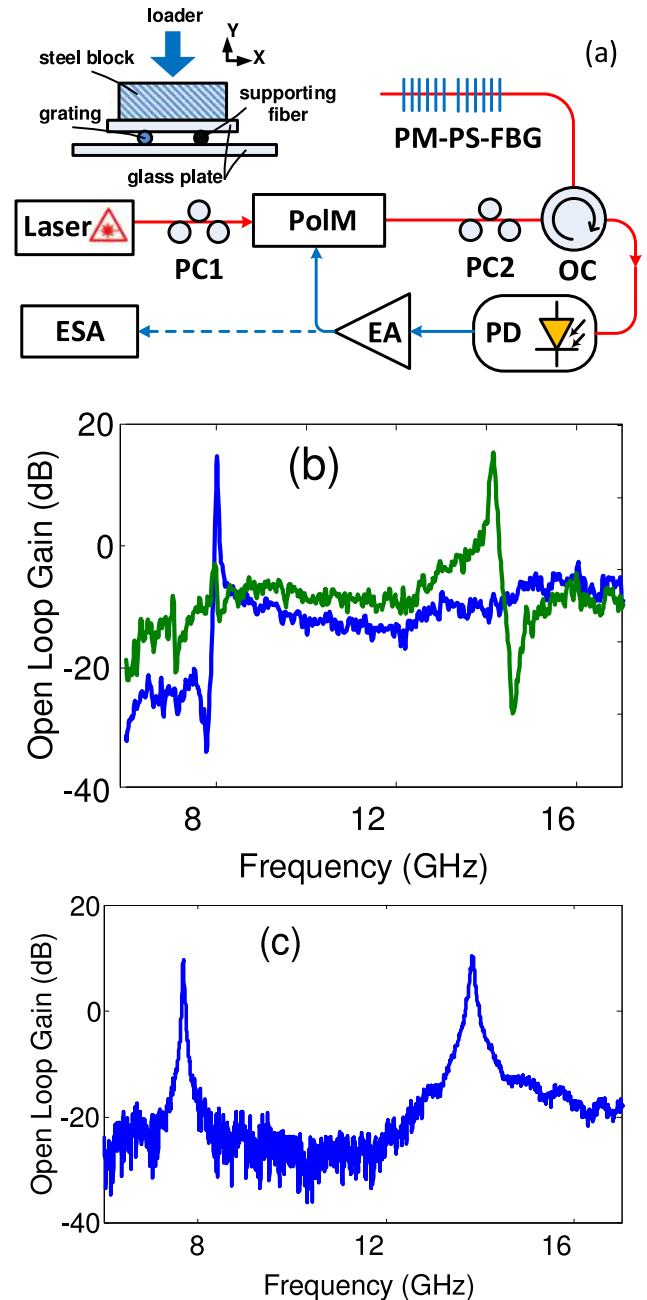


Fig. 8. (a) Schematic of the temperature-insensitive transverse load sensor based on a dual-frequency OEO employing a polarization-maintaining PS-FBG. PolM: polarization modulator; PC: polarization controller; PD: photodetector; EA: electrical amplifier; ESA: electrical spectrum analyzer. (b) Single passband photonic microwave filter when the incident light is aligned with an angle of  $0^\circ$  or  $90^\circ$  relative to one principal axis (horizontal or vertical) of the PolM. (c) Dual passband photonic microwave filter when the incident light is aligned with an angle of  $45^\circ$  relative to one principal axis of the PolM [22].

Then, a transverse load is applied to the polarization-maintaining PS-FBG. To ensure the system reaches to its highest sensitivity and to have a good linearity between the transverse load and the beat frequency, in the experiment the transverse load is applied to the PS-FBG along the fast axis. A supporting fiber with an identical radius is placed in parallel with the polarization-maintaining PS-FBG to make the load being applied to the PS-FBG transversely, while sharing half of the applied load. By

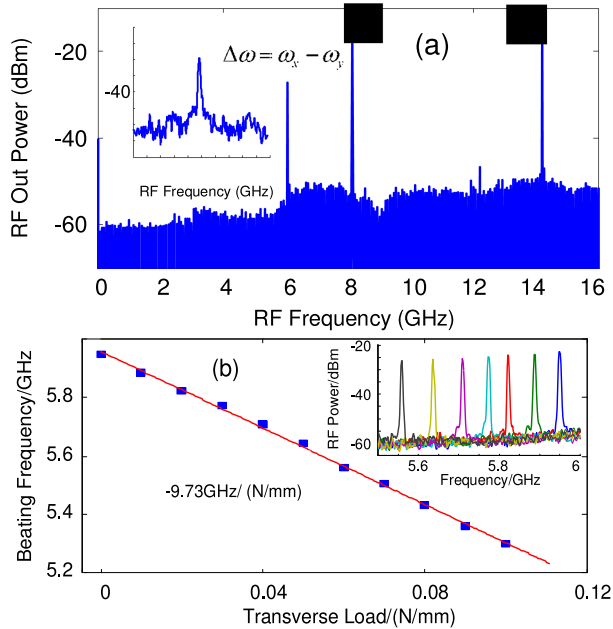


Fig. 9. (a) Electrical spectrum of the signal generated by the dual-frequency OEO, with two microwave signals at 8.22 GHz and 14.24 GHz and a beat signal at 6.02 GHz. (b) Measured beat frequency as a function of the transverse load and the electrical spectrum with different load [22].

increasing the load applied to the polarization-maintaining PS-FBG, the beating frequency is shifted linearly towards a smaller frequency, as shown in Fig. 9(b). The spectrum of the beat signal is measured by an electrical spectrum analyzer (ESA) (Agilent E4448A), with the spectrum shown in the inset of Fig. 9(b). The slope through linear fitting is  $-9.73 \text{ GHz}/(\text{N}/\text{mm})$  which agrees well with the theoretical value of  $9.9 \text{ GHz}/(\text{N}/\text{mm})$ .

By using two independent PS-FBGs, with one as a sensor and the other as a reference, temperature insensitive sensing can also be implemented [23].

The concept was then extended with the light source implemented by a dual wavelength fiber ring laser with improved lasing stability through the use of an injection coupled OEO [24]. The application to transverse load sensing was evaluated. The OEO-coupled dual-wavelength laser has two mutually coupled loops, the fiber ring loop and the OEO loop. In the fiber ring loop, a polarization-maintaining PS-FBG was incorporated to generate two optical wavelengths with the wavelength spacing determined by the birefringence of the PM fiber. In the OEO loop, a microwave signal with its frequency also determined by the birefringence of the PM fiber is generated, which is fed into the fiber ring loop to injection lock the dual wavelengths. Due to the injection locking, a very stable dual-wavelength operation is established. The use of the dual wavelengths for high-resolution and high-speed transverse load sensing was implemented. The sensitivity of the transverse load sensor is measured as high as  $-9.735 \text{ GHz}/(\text{N}/\text{mm})$  and  $+9.754 \text{ GHz}/(\text{N}/\text{mm})$ , along the fast and slow axes, respectively. The high frequency purity and stability of the generated microwave signal permits very reliable and high accuracy measurement and the microwave frequency interrogation allows the system to operate at an ultra-high speed.

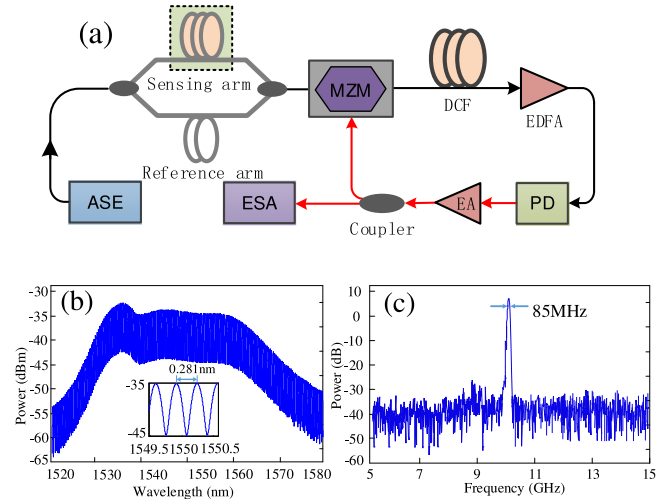


Fig. 10. (a) OEO based sensor based on a MBPF implemented based on a sliced broadband light source. (b) the spectrum of the sliced light source, and (c) The spectral response of the MBPF. ASE: amplified spontaneous emission. MZM: Mach-Zehnder modulator. DCF: dispersion compensating fiber. EDFA: erbium-doped fiber amplifier. PD: photodetector. EA: electrical amplifier. ESA: electrical spectrum analyzer [25].

Instead of using an ultra-narrowband optical filter to implement a MBPF, an OEO-based sensor can also be implemented using a sliced broadband light source [25]. The joint operation of a sliced broadband light source, a Mach-Zehnder interferometer (MZI), a dispersion compensating fiber (DCF), and a PD corresponds to a single passband MBPF [26], as shown in Fig. 10(a) with the spectrum of the sliced light source in (b) and the spectral response of the single passband MBPF in (c). If one arm of the MZI is used as a sensing arm which is exposed to the temperature variations and the other arm is used as a reference arm, when the temperature is changed, the length difference between the two arms is changed, which leads to the change in the free spectral range (FSR) of the MZI. Since the central frequency of the MBPF is a function of the FSR, the oscillation frequency of the OEO is affected by the temperature variations. By measuring the frequency change, the temperature change to the sensing arm is estimated. High sensitivity temperature sensing with a sensitivity of  $3.7 \text{ MHz}/^\circ\text{C}$  was experimentally demonstrated [25].

#### IV. OPTICAL SENSORS BASED ON SPECTRUM SHAPING AND WAVELENGTH-TO-TIME MAPPING

An optical sensor with increased speed and resolution can also be implemented based on optical spectral-shaping and frequency-to-time (SS-WTT) mapping [27], to translate the optical spectrum measurement to the microwave frequency measurement [28], [29]. In addition, through pulse compression, the SNR can also be significantly improved [30], which would increase the measurement accuracy, especially the sensing information is embedded in strong noise.

Optical wavelength-to-time mapping can be performed by using a dispersive element, as shown in Fig. 11. If a dispersive element is a length of fiber with a value of dispersion of  $\Phi$ , for an input pulse  $g(t)$  with a temporal width of  $\Delta t_0$ , the signal at the

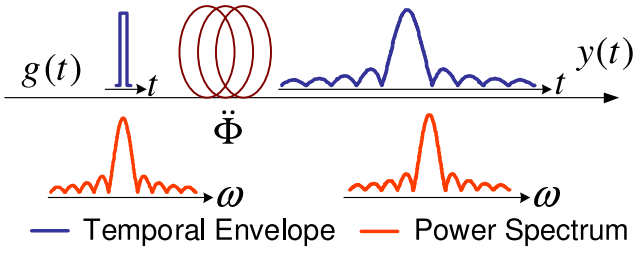


Fig. 11. Wavelength-to-time mapping in a dispersive element.

output of the dispersive element without considering the fiber loss is given [26]

$$\begin{aligned}
 y(t) &= g(t) * \exp\left(j\frac{t^2}{2\ddot{\Phi}}\right) = \int_{-\infty}^{\infty} g(\tau) \times \exp\left[j\frac{(t-\tau)^2}{2\ddot{\Phi}}\right] d\tau \\
 &= \exp\left(j\frac{t^2}{2\ddot{\Phi}}\right) \times \int_{-\infty}^{\infty} g(\tau) \times \exp\left(j\frac{\tau^2}{2\ddot{\Phi}}\right) \\
 &\quad \times \exp\left[-j\left(\frac{t}{\ddot{\Phi}}\right)\tau\right] d\tau \\
 &\approx \exp\left(j\frac{t^2}{2\ddot{\Phi}}\right) \times \int_{-\infty}^{\infty} g(\tau) \times \exp\left[-j\left(\frac{t}{\ddot{\Phi}}\right)\tau\right] d\tau \\
 &= \exp\left(j\frac{t^2}{2\ddot{\Phi}}\right) \times G(\omega)\Big|_{\omega=\frac{t}{\ddot{\Phi}}} \quad (11)
 \end{aligned}$$

where  $G(\omega)$  is the Fourier transform of  $g(t)$ .

As can be seen the envelope of the output signal is proportional to the Fourier transform of the input signal envelope. Note that (11) is obtained if the duration of the input ultrashort pulse,  $\Delta t_0$ , and the dispersion  $\ddot{\Phi}$  of the dispersive element satisfy the condition given by

$$\left|\frac{\Delta t_0^2}{2\ddot{\Phi}}\right| \ll 1 \quad (12)$$

which means that the phase term  $\frac{\tau^2}{2\ddot{\Phi}}$  in (11) satisfies  $\frac{\tau^2}{2\ddot{\Phi}} \leq \frac{\Delta t_0^2}{2\ddot{\Phi}} \ll 1$ , thus we have  $\exp(j\frac{\tau^2}{2\ddot{\Phi}}) \approx 1$ , and  $y(t) \approx G(\frac{t}{\ddot{\Phi}})$ .

Since the pulse compression ratio is determined by the time bandwidth product (TBWP) of a microwave waveform, the microwave waveform should have a large TBWP. A linearly chirp microwave waveform [31] or a random microwave waveform [32] can have a large TBWP. A linearly chirped microwave waveform can be generated optically based SS-WTT mapping in which a spectral shaper with a wavelength dependent FSR that is increasing or decreasing with wavelength is needed.

Fig. 12 shows an optical sensor implemented based on SS-WTT mapping [28]. An LCFBG is incorporated in one arm of a Mach-Zehnder interferometer (MZI). Due to the wavelength dependent nature of the length of the arm with the incorporated LCFBG, the MZI would have a spectral response with an increasing or decreasing FSR. An ultra-short optical pulse with a wide spectrum from a mode-locked laser source is spectrally shaped by the MZI to generate a spectrum with the shape identical to the spectral response of the MZI. The spectrally shaped spectrum is then mapped to the temporal domain by a dispersive element, such as a dispersion compensating fiber (DCF) or an

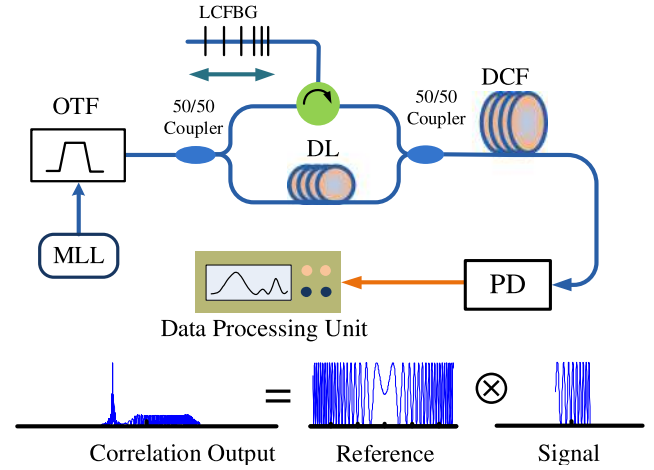


Fig. 12. An optical sensor system based on SS-WTT mapping. MLL: Mode-locked laser; LCFBG: linearly chirped fiber Bragg grating; DL: delay line; DCF: dispersion compensating fiber; PD: photodetector; OTF: optical tunable filter [28].

LCFBG. Due to the linear frequency-to-time mapping, a linearly chirped microwave waveform with a temporal shape identical to the shape of the spectrally shaped spectrum is generated. The chirped waveform is detected by a PD and then sent to a DSP to perform pulse compression.

It is known that a chirped waveform can be compressed if it is sent to a correlator or matched filter in which a reference waveform identical to the chirped waveform is used. The key significance of performing pulse compression is that the wavelength shift is estimated by measuring the location of the correlation peak, with both improved resolution and SNR. The correlation is implemented in the DSP by building a reference microwave waveform, which is linearly chirped with a chirp rate identical to that of the generated chirped microwave waveform, but with an instantaneous frequency extending from the smallest to the largest possible values corresponding to the generated chirped microwave waveform when the LCFBG is experiencing the largest and the smallest wavelength shift. Therefore, the location of the correlation peak would precisely indicate the wavelength shift.

The concept was evaluated by an experiment with the results shown in Fig. 13. A microwave waveform with a chirp rate of  $-0.068$  GHz/ps for  $t < 0$  and  $0.068$  GHz/ps for  $t > 0$  is built as a reference microwave waveform, as shown in Fig. 13(a). Fig. 13(b), (c) and (d) shows three linearly chirped microwave waveforms corresponding to three strains of  $71.5 \mu\epsilon$ ,  $406.9 \mu\epsilon$ , and  $484.2 \mu\epsilon$  applied to the LCFBG, respectively. The correlation of the three linearly chirped microwave waveforms with the reference microwave waveform is shown in Fig. 13(e). The waveforms are highly compressed. The locations of the three peaks indicate the wavelength shifts of the LCFBG are  $0.087$  nm,  $0.495$  nm, and  $0.589$  nm, corresponding to three different strains of  $71.5 \mu\epsilon$ ,  $406.9 \mu\epsilon$ , and  $484.2 \mu\epsilon$ , respectively.

The system could also be modified to have the ability to simultaneously measure the temperature and strain by replacing the single-mode LCFBG to a high-birefringence LCFBG (Hi-Bi



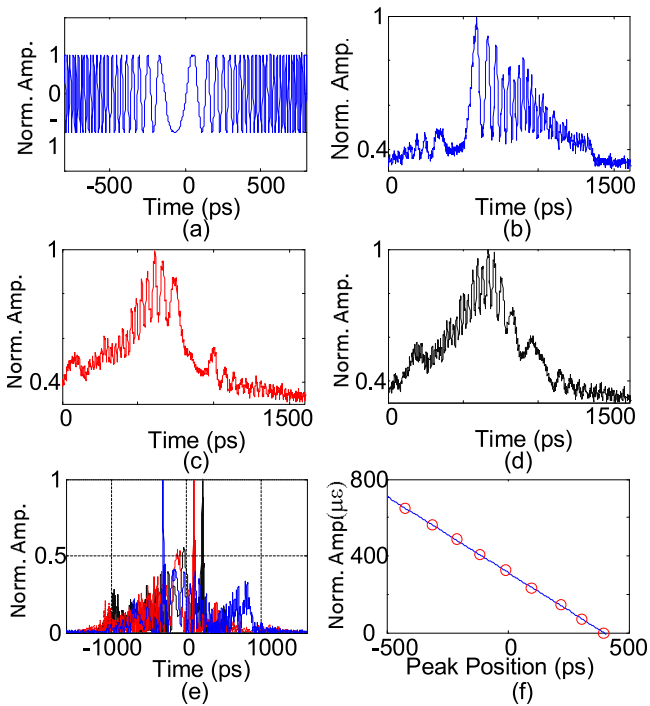


Fig. 13. (a) Reference microwave waveform. (b) Measured chirped microwave waveform when a strain of  $71.5 \mu\epsilon$  is applied to the LCFBG. (c) Measured chirped microwave waveform when a strain of  $406.9 \mu\epsilon$  is applied to the LCFBG. (d) Measured chirped microwave waveform when a strain of  $484.2 \mu\epsilon$  is applied to the LCFBG. (e) Correlation results for the detected microwave waveforms as show in (b), (c) and (d). (f) The measured strain vs the peak position. The circles are the experimental data, and the solid curve is linear fitting of the experimental data [28].

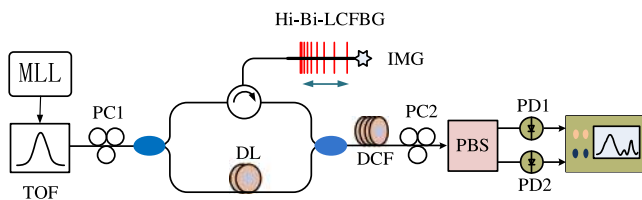


Fig. 14. Schematic of a Hi-Fi LCFBG sensor interrogation system for simultaneous interrogation of temperature and strain. DL: delay line; PBS: polarization beam splitter; DCF: dispersion compensating fiber; IMG: index matching gel; OTF: optical tunable filter; PC: polarization controller [29].

LCFBG), as shown in Fig. 14 [29]. The strain and temperature information are encoded in the Hi-Bi LCFBG as Bragg wavelength shifts along the two orthogonal axes. Due to the birefringence in the Hi-Bi LCFBG, the MZI has two spectral responses along the fast and slow axes with each having an increasing FSR. The spectrum of an ultra-short optical pulse is spectrally shaped by the MZI. Two spectrum-shaped signals are obtained at the output of the MZI which are mapped to two chirped microwave waveforms by a DCF. Again, by pulse compression, two correlation peaks with the locations containing the strain and temperature information are obtained.

The concept was evaluated in which simultaneous temperature and strain measurements were made. Fig. 15(a) shows the reference microwave waveform, and Fig. 15(b) and (c) shows two linearly chirped microwave waveforms corresponding to the two polarization directions of the ultrashort pulses aligned

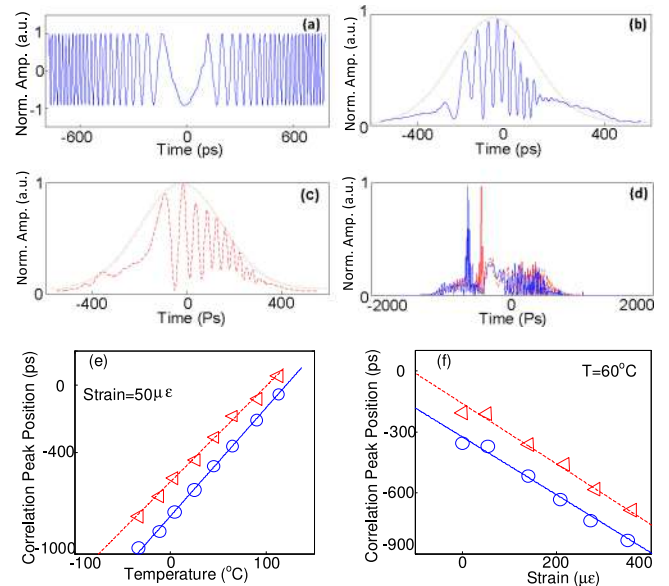


Fig. 15. Experimental results. (a) The reference microwave waveform. A linearly chirped microwave waveform corresponding to the polarization directions of the ultrashort pulse aligned with (b) the fast axis and (c) the slow axis, when a strain of  $50 \mu\epsilon$  is applied to the LCFBG at  $25^\circ\text{C}$ . (d) Correlation of the waveforms in (b) and (c) with the reference waveform. (e) Correlation peak position vs temperature for a given strain of  $50 \mu\epsilon$ . (f) Correlation peak position vs applied strain for a temperature of  $60^\circ\text{C}$ . The triangles and circles indicate the experimental data corresponding to the polarization directions of the ultrashort pulse aligned with the fast axis and slow axis, respectively [29].

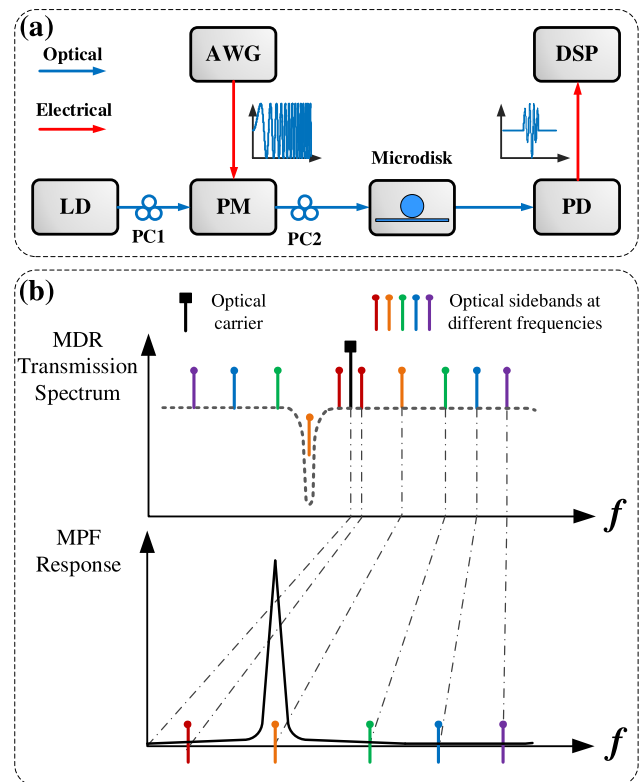


Fig. 16. (a) configuration of the proposed interrogation system; (b) An MPF based on phase modulation to intensity modulation conversion. LD: laser diode; PC: polarization controller; PM: phase modulator; PD: photo detector; AWG: arbitrary waveform generator; DSP: digital signal processor [42].

with the fast and slow axes of the Hi-Bi LCFBG, respectively, when the strain is  $50 \mu\epsilon$  and the temperature is  $25^\circ\text{C}$ . The correlation of the two linearly chirped microwave waveforms with the reference microwave waveform given in Fig. 15(a) is shown in Fig. 15(d). It can be seen the microwave waveforms are significantly compressed. The locations of the two correlation peaks indicate the wavelength shifts of the Hi-Bi LCFBG and the phase difference due to the birefringence of the Hi-Bi fiber. In the experiment, the relationship between the strain, temperature and the correlation peak positions was evaluated, which is shown in Fig. 15(e) and (f).

Note that if a dispersive element has higher order dispersion, the use of the linear wavelength-to-time mapping relationship in (11) would lead to errors and has to be modified. In [33], wavelength-to-time mapping incorporating higher order dispersion for high-speed and high-resolution sensing was proposed and studied.

The use of the concept of optical WTT mapping to convert the spectrum of an FBG filtered by two Gaussian filters to perform high-speed and high-resolution sensing was also reported and demonstrated [34]. The spectrums of the FBG after being filtered by the two Gaussian filters were converted to the time domain via WTT mapping. By comparing the temporal waveforms corresponding to the outputs from the two Gaussian filters, the wavelength shifting information of the FBG was retrieved.

Instead of using a linearly chirped microwave waveform to achieve pulse compression, the use of a random microwave waveform can also achieve effective pulse compression. Recently, a technique to use a random grating serving as a spectral shaper to generate a random microwave waveform based on SS-WTT mapping for high-speed and high-resolution sensing was reported [35]. The experimental results showed that the sensing resolutions for temperature and strain were  $0.23^\circ\text{C}$  and  $2.5 \mu\epsilon$ , respectively, and the accuracies for temperature and strain are  $0.11^\circ\text{C}$  and  $1.2 \mu\epsilon$ , respectively. One added advantage of this approach is that multiple random gratings can be cascaded for remote and distributed sensing. Since each random grating has its unique random spectrum, through pulse compression, a correlation peak representing a specific random grating at a specific location is generated [36].

## V. INTEGRATED MICROWAVE PHOTONIC SENSORS

Silicon photonic devices implemented on a silicon-on-insulator (SOI) platform have a high potential for optical sensing owing to their high sensitivity to refractive index (RI) changes, which is very useful for chemical diagnostics and label-free biosensing since the presence of micro or nano particles on the devices can be detected through measuring the resonant wavelength changes [37]. Numerous SOI-based sensors, such as nanocavity sensors [38], microring resonator sensors [39], microdisk resonator sensors [40], and waveguide Bragg grating sensors [41], have been reported. However, the sensing information encoded in these sensors is obtained through direct wavelength shift measurement by an OSA. Due to low interrogation speed and the poor resolution of an OSA, the performance including sensing speed and resolution is limited. A solution

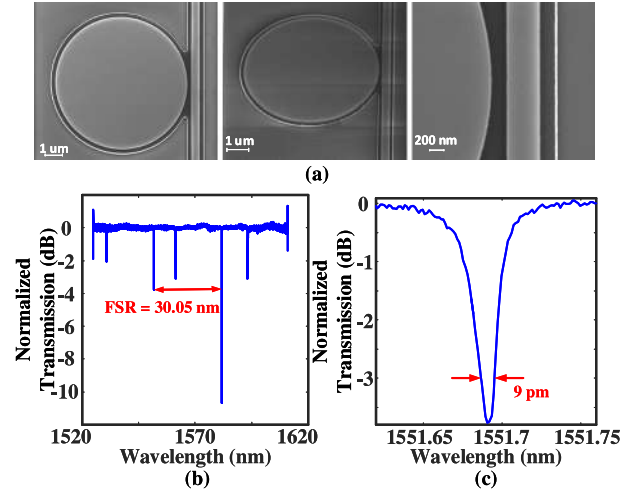


Fig. 17. (a) SEM micrographs of an MDR (with the left picture taken vertically, the middle taken with a tilted angle of  $45^\circ$ , and the right showing the zoom-in view of the gap); (b) normalized transmission spectrum of the fabricated MDR with air cladding; (c) zoom-in view of the  $\text{TE}_0$  mode resonance of the MDR with air cladding [42].

is to use microwave photonics techniques to convert the optical spectrum information to the electrical domain, to measure the microwave spectrum using a DSP.

In [42], a high-speed and high-resolution silicon photonic microdisk resonator (MDR) sensor based on microwave photonic filtering and advanced signal processing was proposed. Fig. 16(a) shows the system configuration. The system consists of a laser diode (LD), a PM, an MDR, and a PD. The integrated MDR with a high Q factor is used as an optical notch filter to filter out one of the sidebands, as shown in Fig. 16(b). The SEM micrographs of the MDR and its transmission spectrum are shown in Fig. 17(a) and (b), respectively. Thanks to the PM-IM conversion in the MDR, a phase-modulated optical signal is converted to an intensity-modulated optical signal, and the entire system is equivalent to a microwave photonic filter with the center frequency of its passband determined by the wavelength of the LD and the notch wavelength of the MDR. Since the center frequency of the microwave photonic filter is a function of the resonant wavelength of the MDR, when the temperature or the RI of the microparticles on the MDR is changed, the center wavelength is shifted, leading to the change of the center frequency of the microwave photonic filter. To effectively measure the spectrum change of the microwave photonic filter, a broadband linearly chirped microwave waveform (LCMW) is applied to the input to generate a filtered microwave waveform. By measuring the temporal location of the filtered microwave waveform, the sensing information is revealed.

The resonant wavelength of an MDR can be expressed as [43]

$$\lambda_{res} = \frac{2\pi R}{m} n_{eff} \quad (13)$$

where  $R$  is the disk radius,  $m$  is the mode order and  $n_{eff}$  is the effective index of the guided mode in the waveguide. When the environmental temperature changes, the effective RI will change due to the thermo-optic effect, and the radius will also change due to the thermal expansion effect. Therefore, the

overall wavelength shift is given by [44]

$$\Delta\lambda_{Temp} = \frac{\lambda_{res}}{n_g} \Delta T \left( \alpha_{si} n_{eff} + \frac{\partial n_{eff}}{\partial T} \right) \quad (14)$$

where  $n_g$  is the group index of the guided mode,  $\Delta T$  is the temperature change,  $\alpha_{si}$  is the thermal expansion coefficient and  $\partial n_{eff}/\partial T$  is the thermo-optic coefficient.

When the RI of the cladding ( $n_{clad}$ ) changes, the effective index of the guided mode will also change, which would lead to a resonant wavelength shift, which is given by [45]

$$\Delta\lambda_{RI} = \left( \frac{\lambda_{res}}{n_g} \right) \times \Delta n_{clad} \times \left( \frac{\partial n_{eff}}{\partial n_{clad}} \right) \quad (15)$$

where  $\Delta n_{clad}$  is the cladding RI change.

Assuming the wavelength of the optical carrier is  $\lambda_c$ , the central frequency of the microwave photonic filter is given by

$$f_{MPF} \approx \left( \frac{c}{n_{avg}} \right) \times \left| \frac{\lambda_c - \lambda_{res}}{\lambda_c^2} \right| \quad (16)$$

where  $c$  is the velocity of light in vacuum,  $n_{avg}$  is the average refractive index for the optical path consisting of fibers and the silicon waveguides. When the resonant wavelength of the MDR shifts, the central frequency of the microwave photonic filter will change. The frequency change can be expressed as

$$\Delta f_{MPF} = K \Delta\lambda_{res} \quad (17)$$

where  $K = c/(n\lambda_c^2)$  and  $\Delta\lambda_{res}$  is the wavelength shift due to  $\Delta\lambda_{Temp}$  and  $\Delta\lambda_{RI}$ .

Mathematically, for a linearly chirped microwave waveform, the instantaneous frequency of the waveform is given by

$$f(t) = f_0 + \alpha t \quad (18)$$

where  $\alpha$  is again the chirp rate,  $f_0$  is the initial frequency, and  $t$  is the time. When the linearly chirped microwave waveform is fed to an microwave photonic filter, the temporal location of the output waveform is calculated by  $t = (f_{MPF} - f_0)/C$ . The relationship between the wavelength shift of the MDR and the temporal location is given by

$$\Delta t = \left( \frac{K}{C} \right) \Delta\lambda_{res} \quad (19)$$

When the temporal location is measured, using (19) with (14) or (15), the temperature or the RI change can be obtained.

The concept in [42] was extended to enable simultaneous temperature and RI sensing based on a dual-passband microwave photonic filter implemented using two whispering gallery modes of an MDR [46]. Since the two whispering gallery modes are experiencing different wavelength shifts, by measuring the spectral response of the dual-passband microwave photonic filter, to locate the central frequencies of the two passbands, simultaneous temperature and RI sensing was implemented.

## VI. CONCLUSION

Conventionally, an optical sensor is interrogated in the optical domain to monitor the wavelength shift by either using an OSA to measure the optical spectrum or measuring the wavelength-dependent intensity change. The speed is slow, and

the resolution is poor. The use of microwave photonics techniques to translate the optical wavelength change in the optical domain to the microwave frequency change in the electrical domain is a solution to improve both the sensing speed and the resolution. Since a DSP can resolve a microwave frequency with subHz resolution, the sensing resolution is extremely high. On the other hand, a high resolution is achieved at the cost of limited measurement range. For example, if the wavelength of an optical sensor is shifted by 10 nm, the corresponding microwave frequency shift is 1.25 THz, which is too wide to be measured by a low-cost DSP. A solution is to use an optical comb [47] to divide the large frequency range into multiple spectral segments. Via parallel processing, low cost DSPs can handle high-speed and high-resolution measurements over a wide measurement range.

## REFERENCES

- [1] E. Udd, "An overview of fiber-optic sensors," *Rev. Sci. Instrum.*, vol. 66, no. 8, pp. 4015–4030, Aug. 1995.
- [2] A. D. Kersey *et al.*, "Fiber grating sensors," *J. Lightw. Technol.*, vol. 15, no. 8, pp. 1442–1463, Aug. 1997.
- [3] A. Othonos and K. Kalli, *Fiber Bragg Gratings: Fundamentals and Applications in Telecommunications and Sensing*. Norwood: Artech House, 1999.
- [4] J. Albert, L. Y. Shao, and C. Caucheteur, "Tilted fiber Bragg grating sensors," *Laser Photon. Rev.*, vol. 7, no. 1, pp. 83–108, Feb. 2013.
- [5] K. P. Koo and A. D. Kersey, "Bragg grating-based laser sensors systems with interferometric interrogation and wavelength division multiplexing," *J. Lightw. Technol.*, vol. 13, no. 7, pp. 1243–1249, Jul. 1995.
- [6] C. Wang and J. Yao, "Ultrafast and ultrahigh-resolution interrogation of a fiber Bragg grating sensor based on interferometric temporal spectroscopy," *J. Lightw. Technol.*, vol. 29, no. 19, pp. 2927–2933, Oct. 2011.
- [7] H. Xia, C. Zhang, H. Mu, and D. Sun, "Edge technique for direct detection of strain and temperature based on optical time domain reflectometry," *Appl. Opt.*, vol. 48, no. 2, pp. 189–197, Jan. 2009.
- [8] S. M. Melle, K. Liu, and R. M. Measures, "A passive wavelength demodulation system for guided-wave Bragg grating sensors," *IEEE Photon. Technol. Lett.*, vol. 4, no. 5, pp. 516–518, May 1992.
- [9] Y. J. Rao, D. A. Jackson, L. Zhang, and I. Bennion, "Dual-cavity interferometric wavelength-shift detection for in-fiber Bragg grating sensors," *Opt. Lett.*, vol. 21, no. 19, pp. 1556–1558, Oct. 1996.
- [10] J. Yao, "Microwave photonics for high resolution and high-speed interrogation of fiber Bragg grating sensors," *Fiber Integr. Opt.*, vol. 34, no. 4, pp. 230–242, Oct. 2015.
- [11] J. Yao, "Microwave photonics," *J. Lightw. Technol.*, vol. 27, no. 3, pp. 314–335, Feb. 2009.
- [12] B. Guan, L. Jin, Y. Zhang, and H. Tam, "Polarimetric heterodyning fiber grating laser sensors," *J. Lightw. Technol.*, vol. 30, no. 8, pp. 1097–1112, Apr. 2012.
- [13] G. A. Ball, G. Meltz, and W. W. Morey, "Polarimetric heterodyning Bragg-grating fiber-laser sensor," *Opt. Lett.*, vol. 18, no. 22, pp. 1976–1978, Nov. 1993.
- [14] D. Donlagic and M. Lesic, "All-fiber quasi-distributed polarimetric temperature sensor," *Opt. Express*, vol. 14, no. 22, pp. 10245–10254, Oct. 2006.
- [15] X. Lin, Y. Liang, L. Jin, and L. Wang, "Dual-polarized fiber laser sensor for photoacoustic microscopy," *Sensors*, vol. 19, no. 21, pp. 4632, Oct. 2019.
- [16] D. Liu, N. Q. Ngo, S. C. Tjin, and X. Dong, "A dual-wavelength fiber laser sensor system for measurement of temperature and strain," *IEEE Photon. Technol. Lett.*, vol. 19, no. 15, pp. 1148–1150, Aug. 2007.
- [17] E. H. Bernhardt *et al.*, "Intra-laser-cavity microparticle sensing with a dual-wavelength distributed-feedback laser," *Laser Photon. Rev.*, vol. 7, no. 4, pp. 589–598, Apr. 2013.
- [18] Y. Wang, J. Zhang, O. L. Coutinho, and J. Yao, "Interrogation of a linearly chirped fiber Bragg grating sensor with a high resolution using a linearly chirped optical waveform," *Opt. Lett.*, vol. 40, no. 21, pp. 4923–4926, Nov. 2015.
- [19] Z. Meng *et al.*, "Dual-band dechirping LFM CW radar receiver with high image rejection using microwave photonic I/Q mixer," *Opt. Express*, vol. 25, no. 18, pp. 22055–22065, Sep. 2017.

- [20] J. Yao, "Optoelectronic oscillators for high speed and high resolution optical sensing," *J. Lightw. Technol.*, vol. 35, no. 16, pp. 3489–3497, Aug. 2017.
- [21] M. Li, W. Li, J. Yao, and J. Azana, "Femtometer-resolution wavelength interrogation of a phase-shifted fiber Bragg grating sensor using an optoelectronic oscillator," in *Proc. OSA Techn. Dig.*, WA, D.C., USA, 2012, Paper BTu2E.3.
- [22] F. Kong, W. Li, and J. Yao, "Transverse load sensing based on a dual-frequency optoelectronic oscillator," *Opt. Lett.*, vol. 38, no. 14, pp. 2611–2613, Jul. 2013.
- [23] O. Xu, J. Zhang, H. Deng, and J. Yao, "Dual-frequency optoelectronic oscillator for temperature-insensitive interrogation of a FBG sensor," *IEEE Photon. Technol. Lett.*, vol. 29, no. 4, pp. 357–360, Feb. 2017.
- [24] F. Kong, B. Romeira, J. Zhang, W. Li, and J. Yao, "A dual-wavelength fiber ring laser incorporating an injection-coupled optoelectronic oscillator and its application to transverse load sensing," *J. Lightw. Technol.*, vol. 32, no. 9, pp. 1784–1793, May 2014.
- [25] Y. Wang, J. Zhang, and J. Yao, "An optoelectronic oscillator for high sensitivity temperature sensing," *IEEE Photon. Technol. Lett.*, vol. 28, no. 13, pp. 1458–1460, Jul. 2016.
- [26] J. Zhang, L. Gao, and J. P. Yao, "Tunable optoelectronic oscillator incorporating a single passband microwave photonic filter," *IEEE Photon. Technol. Lett.*, vol. 26, no. 4, pp. 326–329, Feb. 2014.
- [27] J. Yao, "Photonic generation of microwave arbitrary waveforms," *Opt. Commun.*, vol. 284, no. 15, pp. 3723–3736, Jul. 2011.
- [28] W. Liu, M. Li, C. Wang, and J. Yao, "Real-time interrogation of a linearly chirped fiber Bragg grating sensor based on chirped pulse compression with improved resolution and signal-to-noise ratio," *J. Lightw. Technol.*, vol. 29, no. 9, pp. 1239–1247, May 2011.
- [29] W. Liu, W. Li, and J. Yao, "Real-time interrogation of a linearly chirped fiber Bragg grating sensor for simultaneous measurement of strain and temperature," *IEEE Photon. Technol. Lett.*, vol. 23, no. 18, pp. 1340–1342, Sep. 2011.
- [30] M. A. Richards, *Fundamentals of Radar Signal Processing*. New York, NY, USA: McGraw-Hill, 2005.
- [31] W. Li and J. Yao, "Generation of linearly chirped microwave waveform with an increased time-bandwidth product based on a tunable optoelectronic oscillator and a recirculating phase modulation loop," *J. Lightw. Technol.*, vol. 32, no. 20, pp. 3573–3579, Oct. 2014.
- [32] H. Deng and J. Yao, "Photonic generation of pseudo random microwave waveform based on a random fiber grating," in *Proc. Opt. Fiber Commun. Conf.*, 2018, Paper W2A.37.
- [33] H. Xia, C. Wang, S. Blais, and J. Yao, "Ultrafast and precise interrogation of fiber Bragg grating sensor based on wavelength-to-time mapping incorporating higher order dispersion," *J. Lightw. Technol.*, vol. 28, no. 3, pp. 254–261, Feb. 2010.
- [34] M. P. Fernández, L. A. Bulus Rossini, J. L. Cruz, M. V. Andrés, and P. A. Costanzo Caso, "High-speed and high-resolution interrogation of FBG sensors using wavelength-to-time mapping and Gaussian filters," *Opt. Express*, vol. 27, no. 25, pp. 36815–36823, Dec. 2019.
- [35] H. Deng, P. Lu, S. Mihailov, and J. Yao, "High-speed and high-resolution interrogation of a strain and temperature random grating sensor," *J. Lightw. Technol.*, vol. 36, no. 23, pp. 5587–5592, Dec. 2018.
- [36] J. Liu, P. Lu, S. J. Mihailov, M. Wang, and J. Yao, "Real-time random grating sensor array for quasi-distributed sensing based on wavelength-to-time mapping and time-division multiplexing," *Opt. Lett.*, vol. 44, no. 2, pp. 379–382, Jan. 2019.
- [37] P. Prabhathan, V. M. Murukeshan, Z. Jing, and P. V. Ramana, "Compact SOI nanowire refractive index sensor using phase shifted Bragg grating," *Opt. Express*, vol. 17, no. 17, pp. 15330–15341, Aug. 2009.
- [38] J. Jágerská, H. Zhang, Z. Diao, N. L. Thomas, and R. Houdré, "Refractive index sensing with an air-slot photonic crystal nanocavity," *Opt. Lett.*, vol. 35, no. 15, pp. 2523–2525, Aug. 2010.
- [39] K. De Vos, I. Bartolozzi, E. Schacht, P. Bienstman, and R. Baets, "Silicon-on-insulator microring resonator for sensitive and label-free biosensing," *Opt. Express*, vol. 15, no. 12, pp. 7610–7615, Jun. 2007.
- [40] G. A. Rodriguez, S. Hu, and S. M. Weiss, "Porous silicon ring resonator for compact, high sensitivity biosensing applications," *Opt. Express*, vol. 23, no. 6, pp. 7111–7119, Mar. 2015.
- [41] V. M. N. Passaro, R. Loiacono, G. D'Amico, and F. De Leonardis, "Design of Bragg grating sensors based on sub micrometer optical rib waveguides in SOI," *IEEE Sensors J.*, vol. 8, no. 9, pp. 1603–1611, Sep. 2008.
- [42] H. Deng, W. Zhang, and J. Yao, "High-speed and high-resolution interrogation of a silicon photonic microdisk sensor based on microwave photonic filtering," *J. Lightw. Technol.*, vol. 36, no. 19, pp. 4243–4249, Oct. 2018.
- [43] W. Bogaerts *et al.*, "Silicon microring resonators," *Laser Photon. Rev.*, vol. 6, no. 1, pp. 47–73, Sep. 2011.
- [44] G.-D. Kim *et al.*, "Silicon photonic temperature sensor employing a ring resonator manufactured using a standard CMOS process," *Opt. Express*, vol. 18, no. 21, pp. 22215–22221, Oct. 2010.
- [45] J. J. Ackert *et al.*, "Defect-mediated resonance shift of silicon-on-insulator racetrack resonators," *Opt. Express*, vol. 19, no. 13, pp. 11969–11976, Jun. 2011.
- [46] J. Liu, H. Deng, W. Zhang, and J. Yao, "On-chip sensor for simultaneous temperature and refractive index measurements based on a dual-passband microwave photonic filter," *J. Lightw. Technol.*, vol. 36, no. 18, pp. 4099–4105, Sep. 2018.
- [47] J. L. Hall and J. Ye, "Optical frequency standards and measurement," *IEEE Trans. Instrum. Meas.*, vol. 52, no. 2, pp. 227–231, Apr. 2003.

**Jianping Yao** (Fellow, IEEE) received the Ph.D. degree in electrical engineering from the Université de Toulon et du Var, Toulon, France, in 1997. He is a Distinguished University Professor and the University Research Chair with the School of Electrical Engineering and Computer Science, University of Ottawa, Ottawa, ON, Canada. From 1998 to 2001, he was an Assistant Professor with the School of Electrical and Electronic Engineering, Nanyang Technological University, Singapore. In 2001, he joined as an Assistant Professor, the School of Electrical Engineering and Computer Science, University of Ottawa, where he was promoted to an Associate Professor in 2003, and to a Full Professor in 2006. He was appointed the University Research Chair in microwave photonics in 2007. In 2016, he was conferred the title of the Distinguished University Professor at the University of Ottawa. From 2007 to 2010 and from 2013 to 2016, he was the Director of the Ottawa-Carleton Institute for Electrical and Computer Engineering. He has authored or coauthored more than 600 research papers including more than 360 papers in peer-reviewed journals and more than 260 papers in conference proceedings. He is the Editor-in-Chief of the *IEEE Photonics Technology Letters*, a former Topical Editor of the *Optics Letters*, an Associate Editor for the *Science Bulletin*, a Steering Committee Member of the IEEE JOURNAL OF LIGHTWAVE TECHNOLOGY, and an Advisory Editorial Board Member of the *Optics Communications*. He was a Guest Editor of a Focus Issue on Microwave Photonics in the *Optics Express* in 2013, the Lead-Editor of a Feature Issue on Microwave Photonics in the *Photonics Research* in 2014, and a Guest Editor of a Special Issue on Microwave Photonics in the IEEE/OSA JOURNAL OF LIGHTWAVE TECHNOLOGY in 2018. He is currently the Technical Committee Chair of the IEEE MTT-3 Microwave Photonics and an elected Member of the Board of Governors of the IEEE Photonics Society from 2019 to 2021. He was a member of the European Research Council Consolidator Grant Panel in 2016 and 2018, the Qualitative Evaluation Panel in 2017, and a Panelist of the National Science Foundation Career Awards Panel in 2016. He was also the Chair of a number of international conferences, symposia, and workshops, including the Vice Technical Program Committee (TPC) Chair of the 2007 IEEE Topical Meeting on Microwave Photonics, TPC Co-Chair of the 2009 and 2010 Asia-Pacific Microwave Photonics Conference, TPC Chair of the high-speed and broadband wireless technologies subcommittee of the IEEE Radio Wireless Symposium from 2009 to 2012, TPC Chair of the microwave photonics subcommittee of the IEEE Photonics Society Annual Meeting 2009, TPC Chair of the 2010 IEEE Topical Meeting on Microwave Photonics, General Co-Chair of the 2011 IEEE Topical Meeting on Microwave Photonics, TPC Co-Chair of the 2014 IEEE Topical Meetings on Microwave Photonics, General Co-Chair of the 2015 and 2017 IEEE Topical Meeting on Microwave Photonics, and the General Chair of the 2019 IEEE Topical Meeting on Microwave Photonics. He was a Committee Member for a number of international conferences, such as IPC, OFC, CLEO, BGPP, and MWP. He was the recipient of the 2005 International Creative Research Award of the University of Ottawa, the 2007 George S. Giinski Award for Excellence in Research, the 2017–2018 Award for Excellence in Research of the University of Ottawa, and the 2018 R.A. Fessenden Silver Medal from IEEE Canada. In 2008, he was awarded a Natural Sciences and Engineering Research Council of Canada Discovery Accelerator Supplements Award. He was selected as the recipient of an inaugural OSA Outstanding Reviewer Award in 2012 and was one of the top 10 reviewers of IEEE/OSA JOURNAL OF LIGHTWAVE TECHNOLOGY 2015–2016. He was an IEEE MTT-S Distinguished Microwave Lecturer from 2013 to 2015. He is a registered Professional Engineer of Ontario. He is a Fellow of the Optical Society of America, the Canadian Academy of Engineering, and the Academy of Science of the Royal Society of Canada.